The Astrophysical Journal, 884:18 (12pp), 2019 October 10 https://doi.org/10.3847/1538-4357/ab3a98
© 2019. The American Astronomical Society. All rights reserved.

Can an Unobserved Concentration of Magnetic Flux Above the Poles of the Sun Resolve the Open Flux Problem?

Pete Riley, Jon A. Linker, Zoran Mikic, Ronald M. Caplan, Cooper Downs, and Jean-Luc Thumm
Predictive Science Inc., 9990 Mesa Rim Road, Suite 170, San Diego, CA, USA; pete@predsci.com
Received 2019 July 26; revised 2019 August 8; accepted 2019 August 8; published 2019 October 8

Abstract

Global models of the extended solar corona, driven by observed photospheric magnetic fields, generally cannot reproduce the amplitude of the measured interplanetary magnetic field at 1 au (or elsewhere in the heliosphere), often underestimating it by a factor of two or more. Some modelers have attempted to resolve this "open flux" problem by adjusting what they believe to be errors in the estimates of the photospheric field values. Others have simply multiplied interplanetary estimates by some correction factor to match 1 au values. Here, we investigate whether this "missing" flux can be explained by a source of largely unobserved, concentrated bundles of flux in the photosphere at latitudes too high to be adequately resolved by ground-based observatories or Earth-based spacecraft. Using potential field source-surface and magnetohydrodynamic models, we demonstrate that this additional polar flux can (at least partially) resolve the open flux problem, without generating any new observational discrepancies. For example, we show that model solutions without this additional flux systematically produce streams lying at higher hello-latitudes than is inferred from observations. More importantly, adding this polar flux to the models does not substantially change the location or size of computed coronal holes. The upcoming joint ESA/NASA *Solar Orbiter* mission may be able to support or refute this idea.

Unified Astronomy Thesaurus concepts: Solar coronal holes (1484); Interplanetary magnetic fields (824); Solar coronal streamers (1486); Solar photosphere (1518); Magnetohydrodynamical simulations (1966)

1. Introduction

The interplanetary magnetic field (IMF) measured in situ at 1 au (and elsewhere) is the extension of the magnetic field observed in the photosphere, dragged out by the super-Alfvénic solar wind. In the more than 40 yr of overlapping observations, many coronal phenomena have been connected with their interplanetary counterparts. Coronal mass ejections (CMEs) are one such example (e.g., Gosling 1997; Riley et al. 2008). Additionally, in the absence of any obviously transient phenomena, global models of the corona and inner heliosphere have generally been able to reproduce many of the features of the corona and ambient solar wind, and connect them together. However, an enduring problem, and one that is seen across a wide range of models, is that the modeled strength of the IMF, that is, the open magnetic flux, is underestimated, often by a significant factor of 2–3 (e.g., Riley et al. 2012; Linker et al. 2017; Wallace et al. 2019).

The relationship between the amount of computed open flux in the corona and the measured radial component of the IMF at Earth can be written as

$$|B_r^{\rm Earth}| = \frac{|\Phi_{\rm open}|}{4\pi r_E^2} = \frac{1}{4\pi}\left(\frac{R_{ss}}{215R_s}\right)^2 \int |B_r(R_{ss},\,\theta,\,\phi)|d\Omega, \quad (1)$$

where ϕ denotes longitude, R_s is the radius of the Sun, R_{ss} is the radius of a reference source surface (typically 2.0–2.5R_s for potential field source-surface models (PFSSs) or 20–30R_s for magnetohydrodynamic (MHD) models), r_E is the heliocentric distance of the Earth, and the solid-angle integral is computed over a sphere at the source surface. This relationship is supported by *Ulysses* observations showing that the magnitude of the radial component of the IMF is largely independent of latitude (Balogh et al. 1995) but requires that comparisons between the open flux and radial IMF occur on the timescale of a solar rotation or more, since the model solutions are produced from Carrington maps that required that length of time to assemble.

In an earlier study (Linker et al. 2017, herein referred to as Paper I), we addressed the issue of this so-called "open flux problem" by focusing on two important constraints for the models: (1) the open field regions predicted by the models should correspond to the inferred locations of coronal holes from emission measurements; and (2) the open flux predicted by the models should match what is observed at 1 au. Using both PFSS and MHD model results, we focused our analysis on a period surrounding 2010 July, which occurred shortly after solar minimum (2009 January), and which was an interval devoid of any obvious transient activity. We found that we could not simultaneously match the open flux at 1 au and the locations of the coronal hole boundaries. In particular, solutions that approached a good match with the open flux at 1 au produced coronal holes that were substantially larger than those inferred from emission measurements. Similarly, when model and observation-inferred boundaries appeared to match, there was a mismatch in the open flux at 1 au, with models underestimating measurements by up to a factor of two. We also estimated the open solar flux independently, by computing the total observed magnetic flux within automatically detected coronal holes (Caplan et al. 2016), yielding even larger flux underestimates. We argued that either: (1) the observations used to produce an estimate of the magnetic field in the photosphere were systematically underestimating the actual field; or (2) a large fraction of open flux is not rooted within regions that are dark in emission. With respect to the first idea, while it is not likely that low- and mid-latitude photospheric magnetic field observations are systematically low, given the breadth of observatories, techniques, and processing

approaches, we suggested that it is possible that the polar regions, which are always poorly observed, may be a source of undetected magnetic flux, particularly at solar minimum, when the open flux problem is most pronounced, and when unipolar polar regions are well established.

The polar regions of the Sun are never well observed from observatories confined to near-ecliptic latitudes, even with the $\pm 7^{\circ}25$ maximum offset between the solar equatorial and ecliptic planes. In earlier studies, we extrapolated mid-latitude components poleward using a geometrical prescription (e.g., Riley et al. 2001; Linker et al. 2012). Later, we attempted to retain the available, but noisy observations, by diffusing the flux to improve the signal-to-noise ratio (e.g., Riley et al. 2012). Most recently, we have begun using Air Force data assimilative photospheric flux transport (ADAPT) maps (Arge et al. 2010), which continually ingest new data from mid- and low-latitudes, and allow this flux to migrate self-consistently poleward (e.g., Linker et al. 2017). In principle, such maps may be able to predict what the poles should look like, even in the absence of direct observations. One novel feature of such maps (although likely an artifact of the algorithm and not a physical effect) is the appearance of pockets of strong flux within the otherwise unipolar polar fields. There has also been tantalizing evidence from *Hinode* observations that concentrated small-scale fields are present at higher latitudes (Okunev & Kneer 2004; Tsuneta et al. 2008; Ito et al. 2010). These vertical (radial) fields, which span from 70° to 90° in latitude, were estimated to be as strong as 1 kG, all with the same polarity as the polar region in which they were embedded.

In this study, we test the idea that the "missing" flux (i.e., the deficit between what in situ measurements show and global models suggest) can be explained by a source of magnetic field within the polar regions of the Sun that remains unobserved, and, hence, not incorporated into the model boundary conditions. In the sections that follow, we: (1) describe the models and data used; (2) describe and interpret a set of numerical simulations exploring this idea; (3) propose and test several predictions of this idea; and (4) discuss the implications of this study.

2. Methods

2.1. Models

In this study, we employ both PFSS and MHD models to reconstruct the magnetic field in the solar corona, from which we can infer the average open flux at 1 au. Our PFSS model solves Laplace's equation using a finite difference scheme in all three dimensions (Riley et al. 2006; Caplan et al. 2017). The radial component of the magnetic field is specified at the inner boundary ($1R_S$), which we take to be the photospheric surface. At the outer radial boundary, which can be arbitrarily specified, the field is required to become radial. Typically, this "source-surface" radius is set to between 2.0 and $2.5R_S$, the latter value chosen by Hoeksema et al. (1983), at least in part, so that the predicted open flux at 1 au matched in situ measurements.

Our MHD model, Magnetohydrodynamic Algorithm outside a Sphere (MAS), is a fully parallelized resistive algorithm that solves the usual set of equations in spherical coordinates. The method of solution, including the boundary conditions, has been described previously (Mikić & Linker 1994; Linker & Mikić 1997; Linker et al. 1999; Lionello et al. 1999; Mikić et al. 1999; Caplan et al. 2017). In its thermodynamic mode of operation (Lionello et al. 2009), the effects of radiation, thermal conduction, coronal heating, and resistive and viscous diffusion are included. In this study, we use both the polytropic and thermodynamic modes, which more than adequately capture the structure of the coronal magnetic field. Moreover, as we will show, our results and their interpretation do not depend on which model is applied.

2.2. Data

For this study, we use data from the Michelson Doppler Imager (MDI) on board the *Solar and Heliospheric Observatory* (*SOHO*) spacecraft (Scherrer et al. 1995). These measurements have been analyzed extensively and, we believe, are likely the most accurate estimate of photospheric magnetic fields, particularly during the 2010 time period. Standard synoptic maps are produced at a resolution of 3600×1440 (longitude×latitude). However, we have previously explored the effects of using data from a large variety of observatories (Riley et al. 2012, 2014; Linker et al. 2017), and we do not believe the results or conclusions discussed here are sensitive to the source of the data. To demonstrate this, we also make use of National Solar Observatory's (NSO's) Vector Spectromagnetograph (VSM) and *Solar Dynamics Observatory*'s Helioseismic and Magnetic Imager (HMI) synoptic maps.

3. Results

To explore the effects of a largely unobserved concentration of polar flux, we consider three aspects: (1) Possible visible signs of its presence; (2) the impact on the large-scale structure of coronal streamers; and (3) the effect on the size and location of coronal holes.

3.1. Visible Consequences of Additional Polar Flux

We consider the well-studied time period surrounding the 2010 July 11 total solar eclipse, which occurred near the end of Carrington rotations 2098, during which time, there was little transient activity. Panels (a) and (d) of Figure 1 summarize our initial estimates for the northern and southern polar regions, respectively. These maps were derived from published MDI synoptic maps where we progressively diffused the data moving poleward to improve the signal-to-noise ratio. These appear reasonable and are consistent with Earth-based observations at this time. The total positive flux across the entire photosphere was 20.0×10^{22} Mx, which balanced the negative flux. In panels (b) and (e), we have added polar fields concentrated into 800 small spots. Each spot was a circular Gaussian with a mean width of 0.0025 rad, a mean strength of 100 G, a standard deviation of 100 G, and distributed randomly within the polar region. The size and distribution of these spots was inspired by *Hinode* observations; however, only in the most general sense. Since the features we are attempting to explore remain largely unobserved, there is little to quantitatively constrain their properties. The total unsigned flux added to each pole was 3.7×10^{22} Mx. This flux was added within a small circle centered on the north and south poles bounded by $\theta = 0.25$ rad. Thus, the equivalent (uniform) polar field in this circle would be $3.7/(1 - \cos(0.25)) \times 2\pi$, or 19 G. After adding the small spots, the net positive/negative flux rose to $\pm 23.7 \times 10^{22}$ Mx. Finally, in panels (c) and (f), we added a single, smooth Gaussian, centered at each pole, with a peak

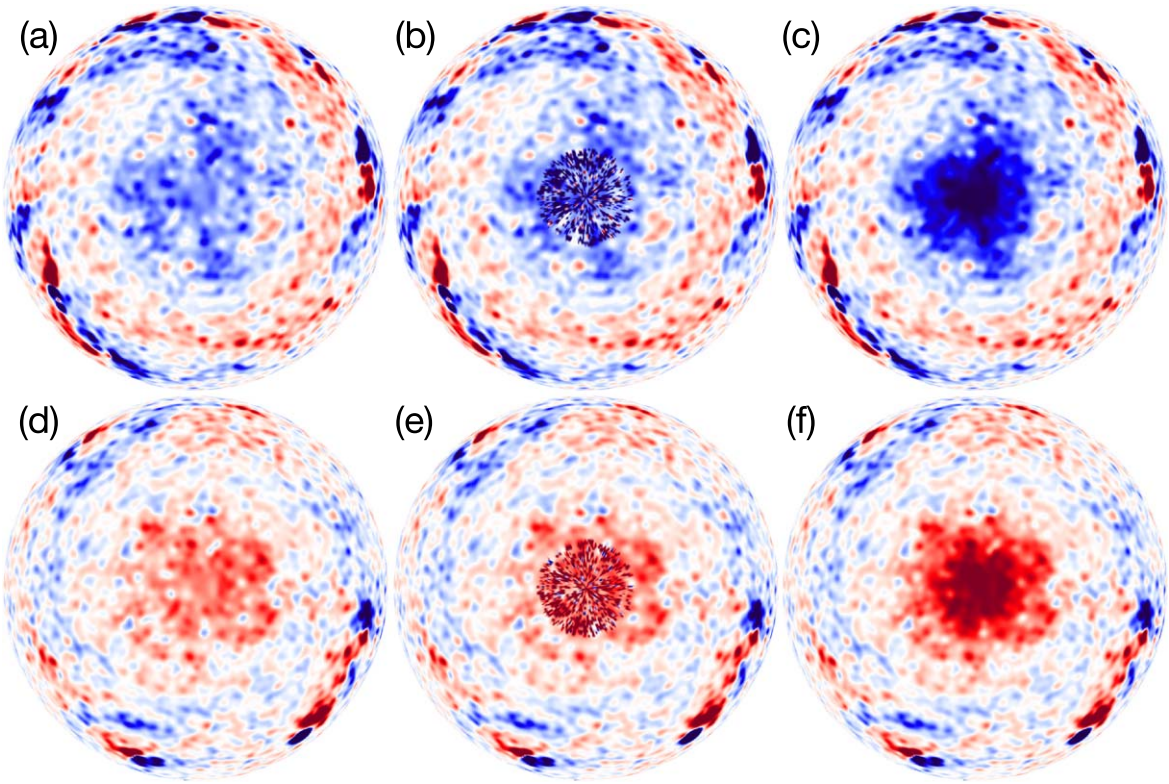

Figure 1. Polar view of the radial component of the photospheric magnetic field for the CR 2097+2098 time period. Panel (a) shows a magnetogram based on standard processing techniques, as viewed from the north pole. Panel (d) shows the same magnetogram as viewed from the south pole. Panels (b) and (e) show the same magnetogram as (a)/(d) but with small-scale polarities (biased toward the sign of the existing field) added to the polar regions. Panels (c) and (f) show the same magnetogram as (a)/(d) but with increased, but smooth polar field contribution.

magnitude of 15G and $\sigma = 0.25$. This resulted in a net positive/negative flux of $\pm 22.86 \times 10^{22}$ Mx. We introduced the "smooth Gaussian" case as a pragmatic simplification of case 2 (b and e). If it can mimic the effects of the small-scale spots, as a practical matter, it would be numerically better suited for MHD calculations.

Using these maps, we computed high-resolution ($101 \times 181 \times 360$) PFSS model solutions for the solar corona. For each case (original flux, small spots, and smooth Gaussian), we then estimated the area of the resulting coronal holes, the open flux at the Sun, and the resulting IMF at 1 au. Table 1 summarizes these results. We note that in moving from the original flux distribution to either of the other two distributions, the coronal hole area change is modest. This is confirmed visually in Figure 2, which shows the computed coronal holes for the three cases. In contrast, the IMF field strength has increased by almost a factor of two (Table 1). These are precisely the changes needed to bring not only our, but other, model results into alignment with observations. We address the potential impacts on the size and location of coronal holes with this additional polar flux in more detail in Section 3.3.

While support for these polar flux concentrations can be found in *Hinode* observations (Tsuneta et al. 2008), a critical question is whether these modifications to the photospheric maps remain consistent with Earth-based observations of the solar magnetic field. Figure 3 addresses this. In panels (a) and (d), we show views from the Earth, assuming that the Earth lies in the solar equatorial plane (i.e., the view at either equinox), such that neither solar pole is preferentially tilted toward Earth. Panel (a) shows the original flux distribution, while (d) shows the modified one, i.e., with small concentrated spots. The main point is that, while a substantial amount of flux was added, which modified the structure of the polar regions as viewed from above each pole, it has a negligible effect as viewed from the Earth. Given the significant increase in the noise component of magnetograms in moving poleward, it is unlikely that we would be able to discern this predominantly transverse signal from Earth's vantage point. Moreover, these projections show the radial component of the field and not the line-of-sight component (which is typically observed). Since the latter decreases substantially moving poleward, these views represent best case scenarios. Even when the Earth is maximally inclined to the solar equatorial plane by 7°.25 (panels (b) and (e)), the conclusions remain unaltered. It would be difficult to identify this structure above the background noise and projection effects that are present. Only with the successful launch of *Solar Orbiter*, with a nominal inclination of 25° and peaking at 34° in the extended mission, would we have the possibility of clearly identifying such features (panel (f)).

Table 1
Estimates of the Area of Coronal Holes (−/+ Polarity), and Open Flux in the Solar Corona and at 1 au

Flux Distribution	Coronal Hole Area (sr)	Open Flux at Sun ($\times 10^{22}$ Mx)	IMF Strength (nT)
Original Flux	−0.629/+0.652	−3.31/+3.31	1.14
Small Spots	−0.586/+0.562	−6.20/+6.20	2.13
Smooth Gaussian	−0.682/+0.672	−5.78/+5.78	1.99

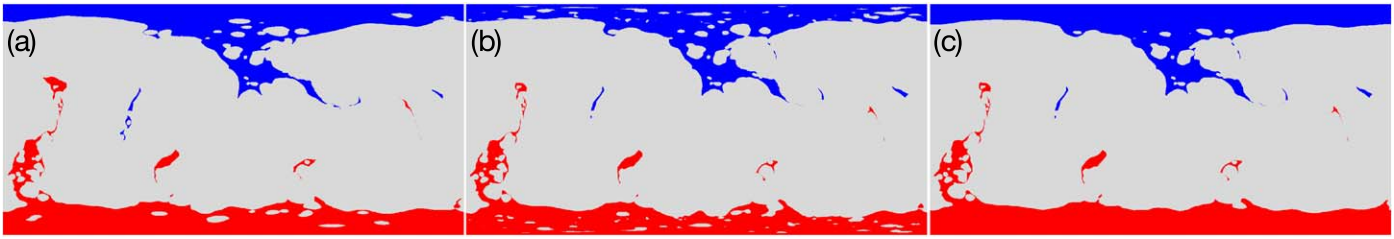

Figure 2. Coronal hole maps for CR 2097+2098, derived using: panel (a) Magnetogram based standard processing; panel (b) same magnetogram as (a), but with small polar spots added; and panel (c) same magnetogram as (a) but with an increased, smooth polar field contribution.

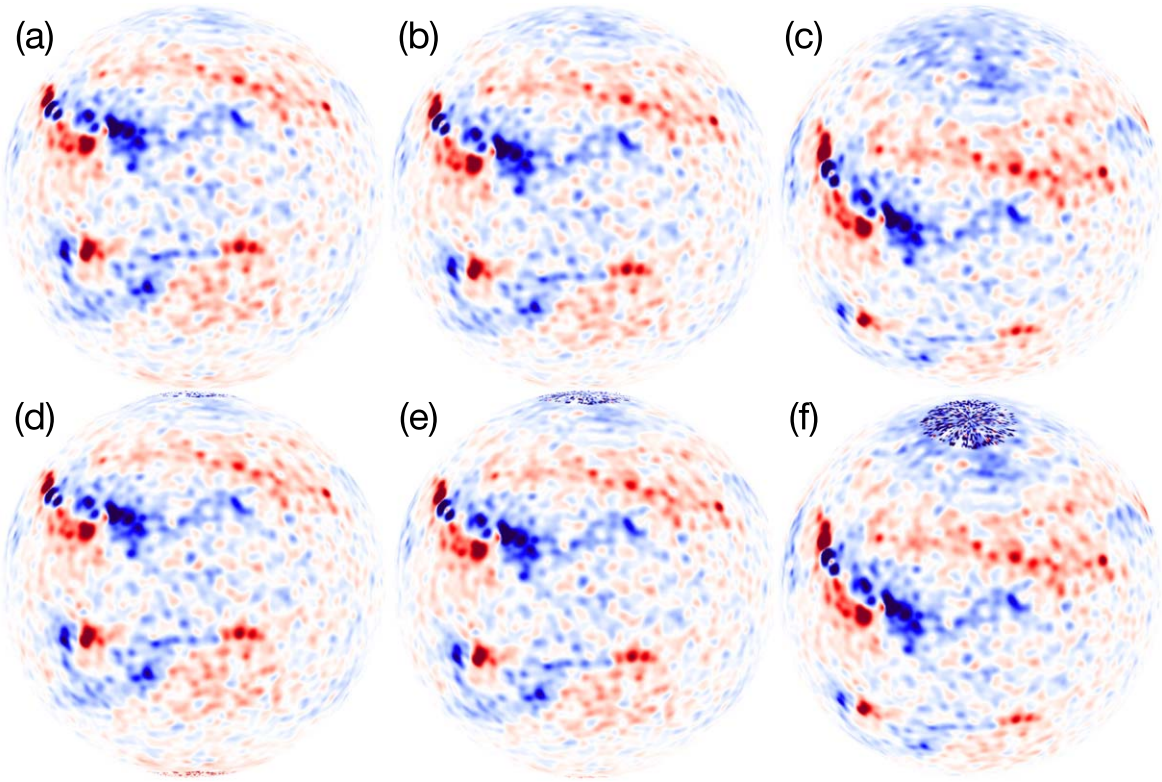

Figure 3. Line-of-sight component of the photospheric magnetic field, centered at Carrington longitude 0°, for different viewing angles (latitudes). Panels (a) and (d) show the view from Earth without and with small spots added to the polar regions, when the Earth is in the solar equatorial plane. Panels (b) and (e) show the same two cases but for when the Earth's position is 7.°25 above the solar equatorial plane. Panels (c) and (f) show the views that *Solar Orbiter* would identify from a vantage point of 30° above the solar equatorial plane.

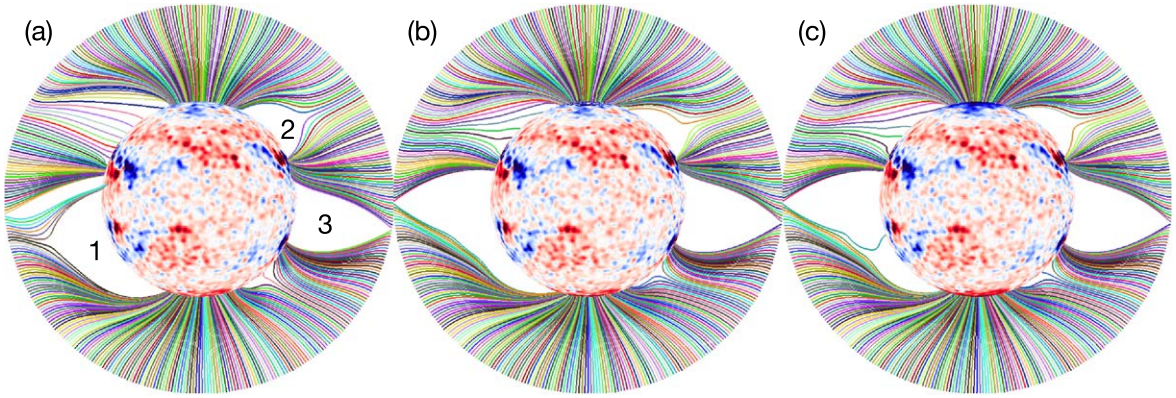

Figure 4. Selection of magnetic field lines drawn from the solar surface to 2 R_S. Panel (a) shows the magnetogram based standard processing. Panel (b) is the same magnetogram as (a) but with parasitic polarities added. Panel (c) is the same magnetogram as (a) but with an increased, smooth polar field contribution.

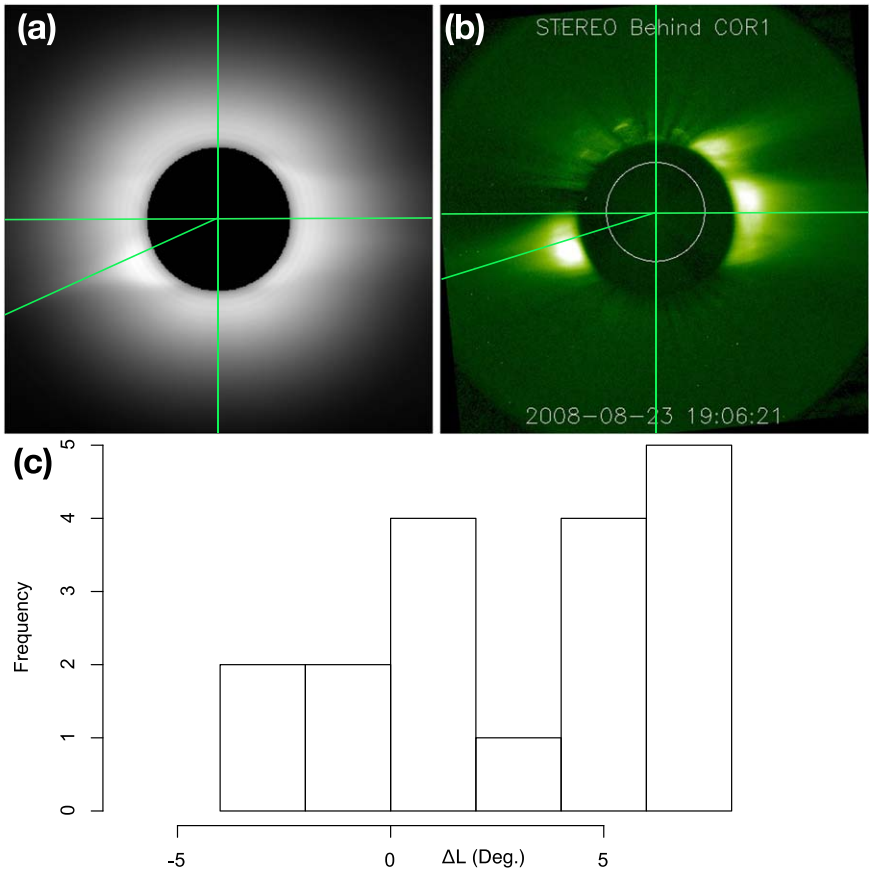

Figure 5. Illustration of how the inclinations of streamer stalks were estimated for: panel (a) the simulated corona, and panel (b) the observed corona, as measured by the COR1 instrument on board *STEREO B*. Panel (c) shows the distribution of the difference between the simulated and observed inclination of the streamer stalks.

3.2. Impact on the Location of Coronal Streamers

If these small-scale polar structures are not obviously inconsistent with current observations, does their presence suggest any testable predictions? One natural consequence is that the extra magnetic pressure produced from the field as it super-radially expands should lead to a transverse, equatorward pressure gradient, which in turn may cause the streamer structure to be pushed equatorward. Figure 4 shows a selection of magnetic field lines drawn from the solar surface (at 1 R_S) out to 2 R_S for the three cases summarized in Table 1. We have marked three streamers (1, 2, and 3). We note that in moving from panel (a) to either panels (b) or (c), the streamer tips move toward the equator, a result of the transverse pressure gradient imposed from the additional polar flux. For streamer 1, this movement is significant ($\sim$18°), while for pseudo-streamer 2 and streamer 3, it is more modest ($\sim$5° and $\sim$3°, respectively).

To investigate this further, we compared the latitudinal extent of simulated streamers from our published thermodynamic MHD model results (PSI 2019) with observed streamers (both dipolar and pseudo (i.e., unipolar) streamers) throughout the period approaching the previous solar minimum (2007 January through 2008 December), during which time the Sun remained relatively quiescent. These simulations were also driven using standard synoptic maps from MDI. In particular, we focused on the latitudinal position of the streamer stalks, which could be quantitatively measured. Since these model results are missing the unseen polar flux, they should predict latitudinal extents that are systematically higher than those observed. We identified candidate streamers for further investigation based on several criteria. First, the interval surrounding them should be generally quiescent. Second, there should be a reasonable match between the simulated and observed images, including the same number of large-scale streamers and a rough correspondence with their position in latitude. During the initial analysis, one of us (P.R.) selected a set of a dozen or so events for analysis, finding that, indeed, the observed streamer stalks were situated at lower latitudes, consistent with our working hypothesis. However, to mitigate the effects of any informed-observer bias, we repeated the analysis with a second analyst (J.L.T.) who: (1) independently identified the best candidate streamers; (2) was not aware of the significance of the measurements; and (3) did not know whether a particular outcome was or was not anticipated. Thus, this represented a single-blind experiment. Figure 5 summarizes the results. In Figure 5(a) and (b), we show an example of the results of measuring the inclination (latitudinal extent, in the plane of the sky) of both simulated and observed streamer stalks. The horizontal lines mark the solar equator, while the angled line in the southwest quadrant is the best estimate for the angular offset from the equator of the tip of the streamer. In this particular case, the simulated stalk lay at a latitude of $S24.^{\circ}1$, while the observed stalk lies at a latitude of $17.^{\circ}3$, consistent with our hypothesis.

The results of this analysis for 20 of the best candidate streamers are shown in Figure 5(c), where ΔL is the difference between simulated and observed stalk inclination. We note the following points. First, there is an asymmetry in the sign of ΔL, with it being strongly positive. Second, there is an asymmetry

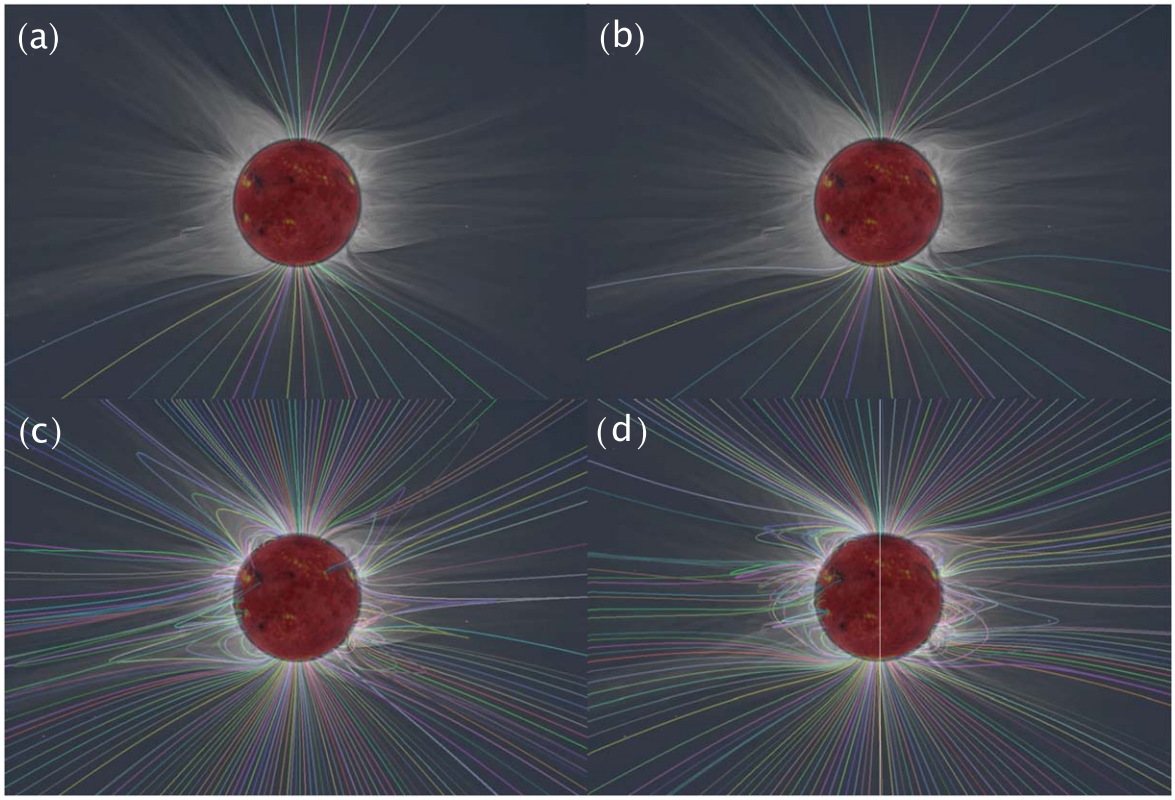

Figure 6. Blended comparison of MHD model results with 2010 eclipse observations by M. Druckmuller and colleagues. In each panel, field lines are shown in arbitrary colors, where the same launch points are used for each specific color, together with white-light observations taken during totality. Panel (a) shows a selection of polar field lines drawn from an MHD solution with no added polar flux. Panel (b) is the same as (a), but with added polar flux. Panel (c) shows a more comprehensive set of field lines are drawn including closed field lines. Panel (d) is the same as (c) but using the MHD solution with added flux.

in the magnitude of ΔL, with positive values being substantially larger than the negative values. The mean value is $3\overset{\circ}{.}1$. Thus, at least subjectively, this suggests that the tips of the simulated streamers tend to lie at higher latitudes than are observed. As a more objective exercise, we also computed a one sample t-test to assess the null hypothesis that this distribution is consistent with a mean equal to zero. The p-value was found to be 0.002, suggesting that we can accept the alternative hypothesis that the true mean is not equal to zero. The 95% confidence interval on the mean was [1.3, 4.9]. Thus, our result suggests that the observed streamer stalks are systematically displaced to lower latitudes than the simulated streamer stalks.

As a second test of what the impact of an undetected concentration of polar flux, might have, we anticipated that the additional magnetic pressure modifies the expansion properties of the magnetic field lines in and surrounding the polar regions, with the solutions incorporating the additional polar flux manifesting larger expansion factors. This can be inferred, at least heuristically from Figure 4. Again, considering the time period surrounding the total solar eclipse of 2010, in Figure 6, we compare two model solutions with eclipse observations made by M. Druckmuller and colleagues (Habbal et al. 2011). In each panel, the white-light observation taken during the eclipse has been blended with a set of field lines from the simulation. Panels (a) and (c) show field lines for an MHD solution that did not include any additional flux, while panels (b) and (d) show the same field lines (that is, traced from the same origin at $1R_S$) for a solution that included additional polar flux. Each row shows a different set of foot-points, with the upper panels including only open field lines from within the polar coronal holes, and the bottom panels showing a more extensive set of field lines that also include streamer and pseudo-streamer structure.

We note several points. First, the addition of polar flux causes the field lines to super-radially expand more. In particular, the gray and blue field lines shown in the N-W and S-W quadrants of panels (a) and (b) are pushed substantially further equatorward. This is apparent with the other field lines both in panels (a) and (b) as well as panels (c) and (d). Second, the large-scale structure of the streamers (panels (c) and (d)) changes significantly with additional polar flux. Given the complexity of viewing structure that is convolved along the line of sight (including the field lines), it is difficult to make definitive statements; however, we can identify regions where the comparison appears to be both improved and worsened with the additional flux. Consider, for example, the pseudo-streamer in the N-E quadrant. In panel (c), the field lines bounding the pseudo-streamer stalk are much more radial than the actual structure observed. In panel (d), however, the stalk has been deflected toward the equator, and closer to the observed trace (perhaps overshooting it). In contrast, however, the helmet streamers in the N-W and S-W quadrants seem to match better with the no-flux-added solution (panel (c)). A closer inspection, however, complicates this interpretation: the two streamers that are more strongly deflected equatorward in panel (d) may in fact align with another pair of streamers (more clearly visible in the white-light images in panels (a) and (b). Third, the orientation of the rays or plumes above the polar regions at least qualitatively match

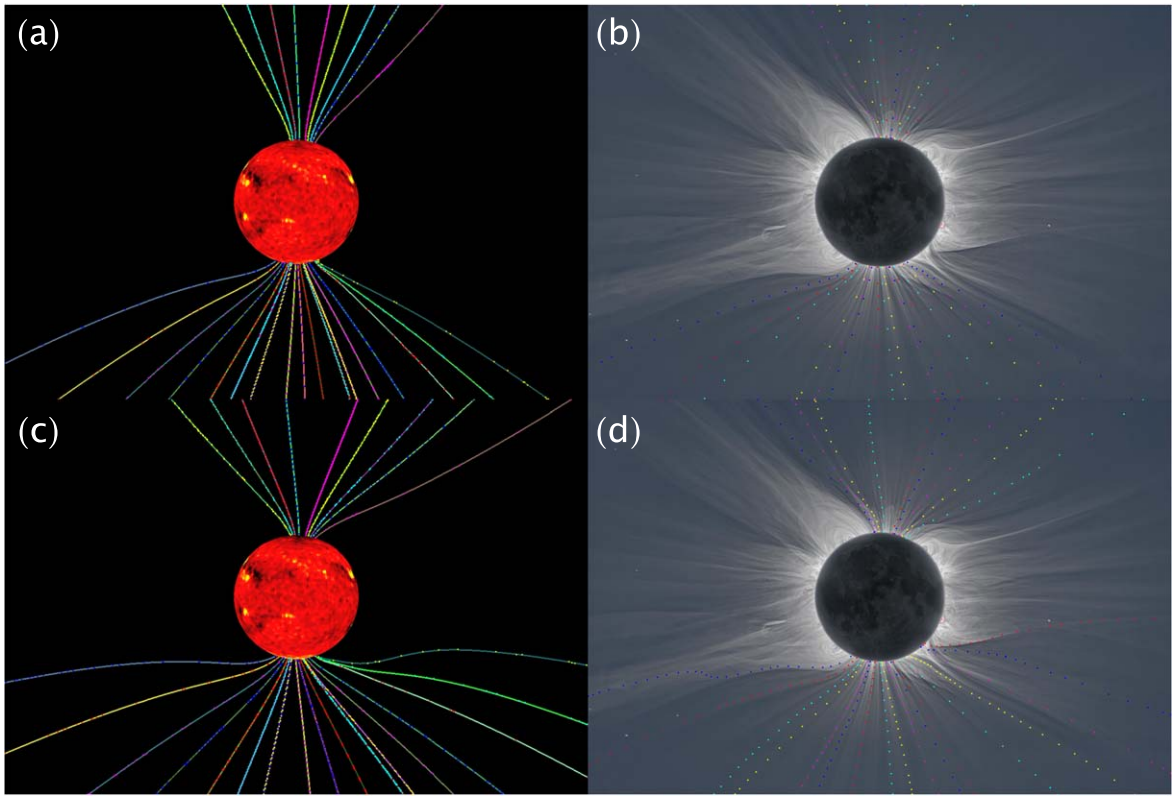

Figure 7. Comparison of MHD model results without (panel (a)) and with (panel (b)) the addition of a concentration of polar flux are compared with an eclipse image (panels (b) and (d)). Field lines have been drawn from a selection of starting points at the base of the corona in (panels (a) and (c)), and the closest, most readily identifiable counterpart to each of them has been identified in the eclipse images (panels (b) and (d)). Each of the dots in the four panels are digitized locations of these traces.

better with the solution containing the added polar flux (see the movie in the supplemental information (SI), which shows a variable-blending of the model results with the eclipse image). Overall, we might tentatively infer that the addition of the polar flux has brought the model results more into alignment with the observations.

To assess the expansion properties of the field lines more quantitatively, we computed effective expansion factors from the white-light observations and the MHD model results for the 2010 solar eclipse. To accomplish this, we identified a set of field lines from each of the model results that originated from the large polar coronal holes. We then attempted to find specific "rays" from the eclipse image that most closely aligned with each of these field lines. For each of these four groups of field lines, we captured the trace of the ray/field line using digitization software. These are summarized in Figure 7. Panel (a) shows MHD model results for the case where no flux was added to the polar regions, while (c) shows field lines drawn from the same starting points at the base of the corona with flux added. The closest matching "rays" from the eclipse image are marked in each of the images in (b) and (d), respectively. Again, to avoid any obvious bias, after an initial exploration of this procedure by one of us (P.R.), the task was assigned to another member of the team (J.L.T.) who had no prior knowledge of the significance of the two MHD solutions or anticipated results.

The digitized representations of each field line were converted to polar coordinates (r, θ), and expansion factors were computed in the following way. For each adjacent field line, the angle $\Delta\Theta$ between them was estimated at two radial distances (r_1 and r_2), $\Delta\Theta_1$ and $\Delta\Theta_2$. To determine the location of the field line at a specific radial distance, a linear interpolation was used between nearest points. The ratio of these angles was used to define an effective expansion factor in two-dimensions. A value of 1 corresponded to radially directed field lines, and values >1 indicated super-radial expansion. Thus, for n field lines, $n-1$ expansion factors were computed. In the cases shown here, $n = 26$ field lines resulted in 25 expansion factors. Figure 8 summarizes the expansion factors computed between $r_1 = 1.25R_S$ and $r_2 = 3.0R_S$. We verified that the results did not depend qualitatively on either of these points by varying each by several fractions of a solar radius. The colored dashed lines represent linear fits to each cluster of points. These are drawn primarily to highlight any vertical offsets between groups of points, and not necessarily to suggest any dependency on latitude. We separated each cluster into positive and negative average (along the traced field line) footpoint clock angles (with zero at each pole), to acknowledge that should any linear trends exist, they would likely reverse sign at, or near the poles.

From Figure 8, we note the following points. First, on average, the expansion factors tend to cluster around four. These values, however, should be interpreted within the context of the starting and end points (1.25 and 3.0, respectively), and not compared directly with other study results, where, for example, the starting and end points may have been different. Second, there is a large amount of scatter for all groups of field lines. This is due to limitations in the procedure for identifying the location of each field line/ray and the linear interpolation between nearest points to estimate values at r_1 and r_2. In

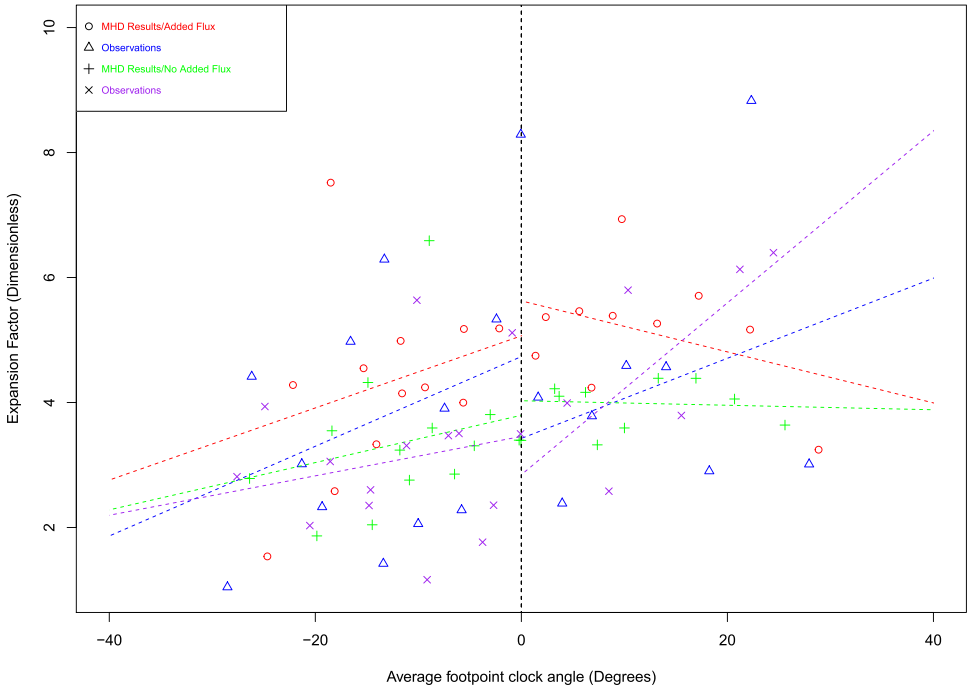

Figure 8. Expansion factors estimated for: MHD results with added flux (red); eclipse observations of rays most closely associated with the MHD solution with added polar flux (blue); MHD results with no added polar flux (green); and eclipse observations of rays nearest the MHD solution with no added flux (purple). The colored dashed lines are linear fits to each cluster of data points, separated into fits for negative and positive footpoint clock angle, which are measured from each pole.

addition, the expansion factor along the flux tubes can evolve in a complex way; thus, the scatter may incorporate nuances in the underlying paths of the field lines. Third, the distribution of points for the MHD solutions without (green) and with (red) added polar flux are separated vertically, suggesting, and as expected, that there is an intrinsic difference in the expansion factors of these field lines. The larger values of the solutions with added flux indicate that these field lines are expanding more than the field lines from the no-added-flux solution. Fourth, the observed field lines from each hemisphere (blue and purple) show no obvious vertical separation; Thus, there are no obvious asymmetries between the hemispheres at this time. Fifth, and unfortunately, the large scatter in the observed field-line expansion factors (blue and purple) largely encompasses the expansion factors from both MHD solutions (red and green). Thus, we conclude that this exercise cannot reliably differentiate between the two model results: Both are consistent with the inferred expansion factors from the eclipse observations.

3.3. Impact on the Size and Location of Coronal Holes

Although relatively under-appreciated, we have known for some time that there exists a fundamental mismatch between the computed areas and locations of coronal holes and their observed counterparts. This is particularly true for PFSS model solutions, where we have found that, in general, to even approach the measured magnitude of the IMF at 1 au, the source-surface radius must be brought in to values well under 2.0 R_S. To assess this more quantitatively, we used photospheric maps from NSO's VSM for CR 2098 as boundary conditions for approximately 40 PFSS solutions, where we set the source-surface radii to different values, ranging from 1.2 to 3.5 R_S, a span that conservatively encompasses all reasonable values that have been contemplated in the past. For each solution, we computed: (1) the total area of the computed coronal holes (strictly, this is the modeled open field area, which may be different from the "coronal hole" area as determined from simulated EUV images) and compared them to the areas estimated from observations (Caplan et al. 2016); and (2) the inferred magnitude of the radial component of the IMF at 1 au.

Figure 9 summarizes these results and highlights several interesting points. First, based on the fractional area difference, a source-surface radius of approximately 1.7 R_S appears to match the observations best (panel (a)). At radii less (greater) than this, the coronal field is too open (closed). Second, based on the observed values of the IMF during CR 2098, the "optimum" source-surface radius must be dropped to values approaching 1.35 R_S (panel (b)). In panel (c), we have combined these two results, which underscores an important result; the model-predicted open flux at 1 au scales linearly with the fractional area difference. Additionally, it highlights the incongruity between the PFSS solutions that best match the coronal hole boundaries and those that best match the open flux at 1 au. Stated another way, for PFSS models to be able to match observations at 1 au, they must produce open field areas that are far too large. Although we have illustrated this effect using PFSS models (given their simplicity), the same problem also arises in the MHD solutions. Finally, to verify that this result was not sensitive to the particular rotation chosen or the source of the synoptic map, we considered HMI LOS synoptic maps for CRs 2189, 2190, 2191, and 2192. During the interval spanned by these rotations, the Sun remained relatively quiescent. In each case, the inferred radial field at 1 au was approximately a factor of two less than in situ measurements, the same as seen for the MDI results.

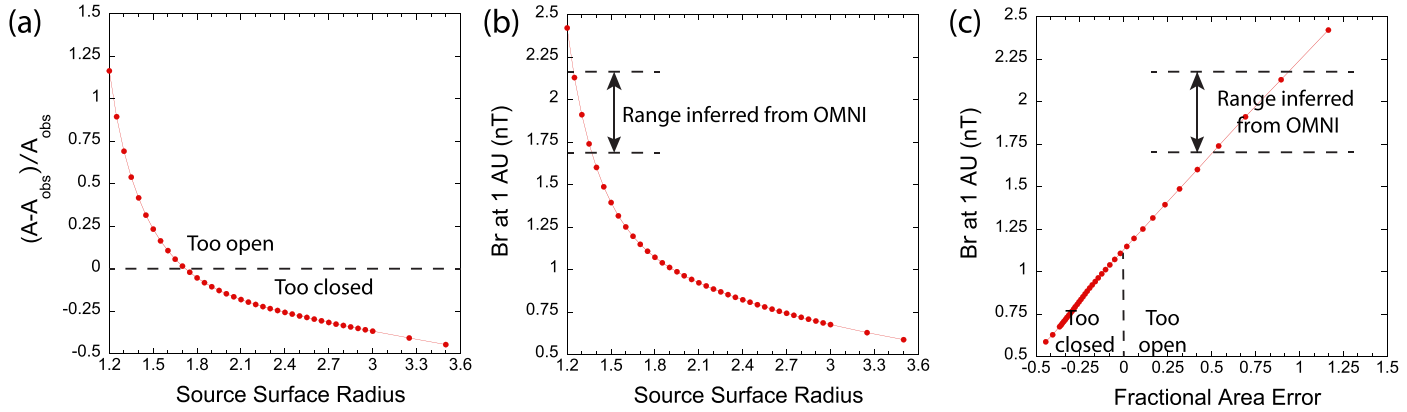

Figure 9. Panel (a) shows the fractional difference in the size of computed coronal holes as a function of source-surface radius. Panel (b) shows the computed open flux at 1 au as a function of the source-surface radius. Panel (c) shows the relationship between the computed open flux at 1 au and the fractional area difference.

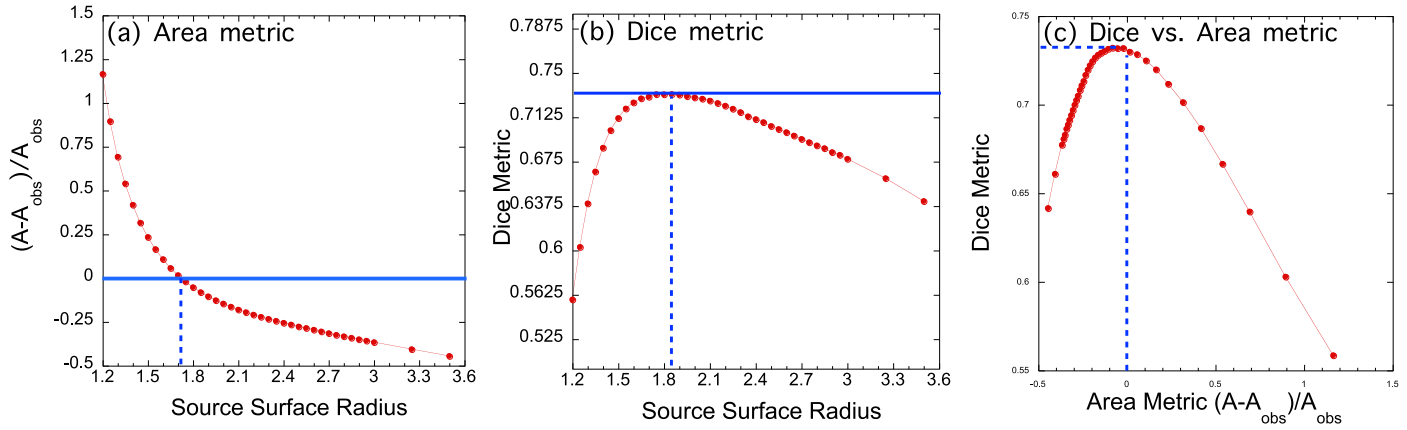

Figure 10. Panel (a) shows the area metric, and panel (b) shows the overlap (dice) metric, as a function of source-surface radius. Panel (c) shows the overlap metric compared to the area metric for each of the PFSS solutions.

The fractional area difference described above is also known as the area metric ($M_{\rm area}$), and is defined by

$$M_{\rm area} = \frac{A_M - A_0}{A_O}, \quad (2)$$

where A_M is the fractional CH area of the modeled Sun, while A_O is the observed CH area. While $M_{\rm area}$ is intuitively appealing, its value is limited because errors in the location of the boundaries are not tracked and thus can cancel. For example, consider an idealized case where only one mid-latitude coronal hole existed on the entire Sun. If the areas of the observed hole and the model hole were the same, but one was in the northern hemisphere and the other in the south, the Area metric would be zero, and the skill score would be 100%, which clearly does not reflect the poor match in this case.

A potentially better metric is the so-called "overlap" or "Dice" metric, which is defined by

$$M_{\rm overlap} = \frac{2A_M \cap A_0}{A_M + A_O} \in [0, 1]. \quad (3)$$

This has the advantage of tracking the differences associated with modeled and observed coronal holes that do not lie on top of one another: when A_M and A_O overlap exactly, $M_{\rm overlap} \rightarrow 1$. Note also that, by convention, $M_{\rm Area}$ and $M_{\rm overlap}$ "improve" in opposite directions: $M_{\rm overlap} \rightarrow 1$ suggests a perfect match between model and observations, while this would be captured (less precisely) by $M_{\rm area} \rightarrow 0$.

Figure 10 illustrates the differences between the two, again for CR 2098. For each PFSS solution, we computed both $M_{\rm area}$ and $M_{\rm overlap}$. As noted above, using $M_{\rm area}$ to rank the solutions resulted in an optimum source-surface value of approximately 1.7 R_S (panel (a)). On the other hand, using the overlap metric resulted in a slightly higher value of 1.85 R_S. How these two radii manifest themselves through the structure of the computed coronal holes is summarized in Figure 11 (panels (b) and (c)). Overall, the differences are modest. However, as shown above, in either case, the computed open flux at 1 au is still significantly below what is observed. By way of comparison, in Figure 11(a), we show the computed coronal hole boundaries for a source-surface radius of 1.35 R_S, which is the value required to produce an open flux at 1 au, that reaches the lower bound of what was observed. Clearly, these open field regions are far too large.

With these considerations in mind, we can now assess what impact adding magnetic flux to the polar regions would have on the shape, size, and location of the coronal holes. Again, we focus on CR 2098. We generated a sequence of PFSS model solutions by adding progressively more magnetic flux, as a Gaussian distribution peaked at each pole. Using a source-surface radius of 1.85 R_S, we stepped through values of 0 to 12.5G of additional flux. Four snapshots are shown in Figure 12, and a movie of the evolution is provided in the Supplemental Information. Adding the equivalent of ~6 G

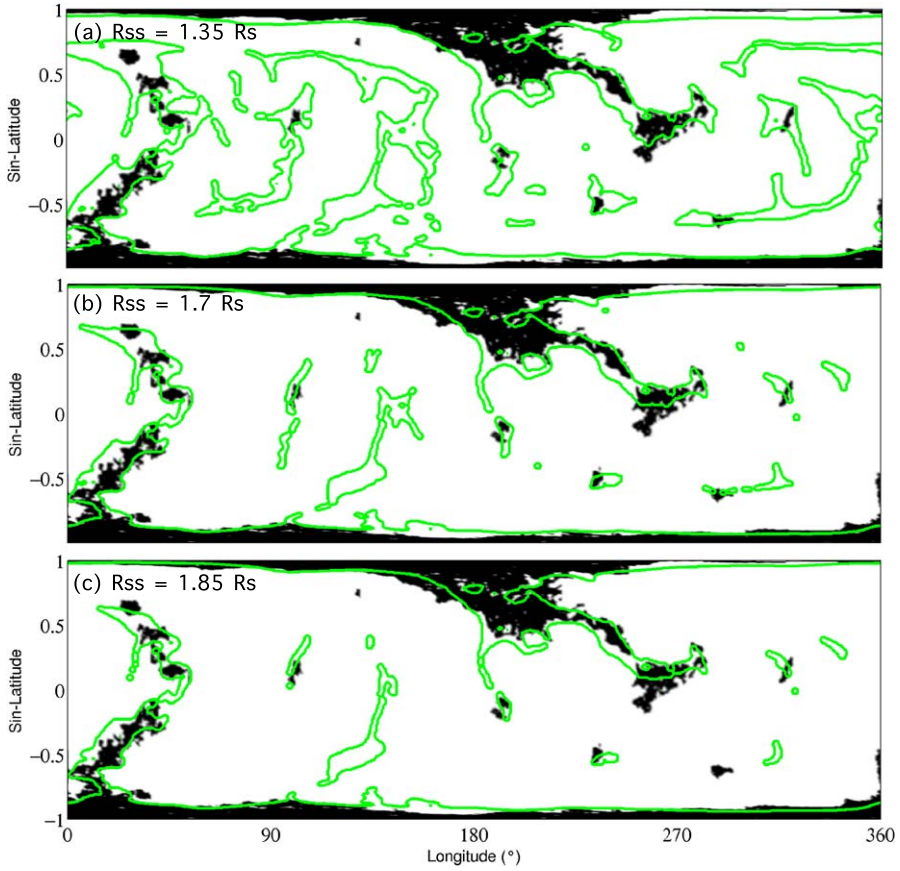

Figure 11. Comparison of observed coronal holes (black regions) to computed coronal holes (green) for CR 2098 for each of three PFSS solutions with different source-surface radii: (a) 1.35 R_S; (b) 1.7 R_S; and (c) 1.85 R_S.

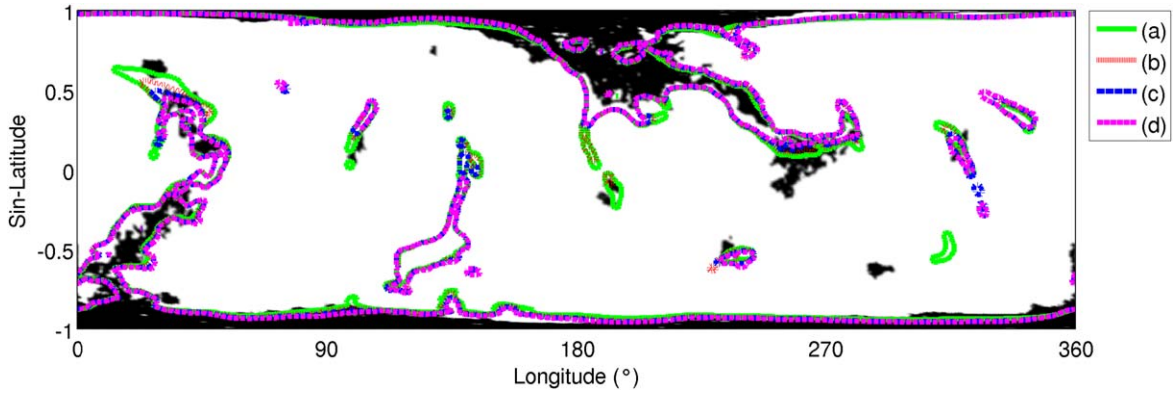

Figure 12. The effects of adding polar flux (a Gaussian distribution centered at each pole) to PFSS models using a source-surface radius of 1.85 R_S. Panel (a) shows no polar flux added; (b) 4.2 G added; (c) 8.3 G added; and (d) 12.5 G added. The observed coronal holes are shown in black, and the computed coronal holes are shown as color contours.

resulted in a computed IMF of ∼1.7 nT, which lies at the lower bound of what was observed by OMNI spacecraft during this time period. This resulted in polar regions with a total flux of approximately 9.5 G, which was 2.7 times the polar flux in the original NSO VSM map. Although this is substantial, based on the analysis in Section 3.1, it may not be inconsistent with our limited Earth-based view.

Using the fraction area metric as the basis for the optimal source-surface radius (1.7 R_S), we repeated the same analysis. Since this smaller radius already resulted in higher computed values of B_r at 1 au, only an additional 5 G of polar flux was required to produce an IMF of 1.7 nT. This resulted in poles with a total flux of 8.5G, or 2.4 times the flux in the original NSO maps. While less than the previous increase, it is not insignificant. On the other hand, again, it is not likely inconsistent with our current, limited observations of the poles.

As a final numerical experiment, we again computed a set of PFSS solutions, however, limiting the increase in the amplitude of the polar flux to approximately double the observed value. This would lead to a computed open flux at 1 au of 1.54 nT. Although this does not entirely bridge the gap, it brings the modeled IMF substantially closer to what is observed, and, importantly, is consistent with *Hinode* observations.

4. Summary and Discussion

In this study, building on the results of Paper I, we have explored the hypothesis that the "missing" solar flux, that is, the deficit between the flux measured at 1 au and that estimated from global models of the solar corona, can be provided by a largely unobserved source of flux hidden near the poles of the Sun. We tested this idea by adding distributions of flux to the polar regions and comparing the resulting estimates at 1 au with observations, finding that such a scenario, while not obviously violating any observational constraints (coronal hole areas and structure), can account for at least a substantial fraction of the missing flux at 1 au. We also considered two potential ramifications of the presence of this polar flux. First, there should be a net offset in the latitudinal extent of coronal streamer stalks between observations and model results that did not incorporate the additional flux, with the observed stalks being pushed further toward the equator than the simulated stalks, consistent with the idea of additional latitudinal pressure gradients set up by the additional flux. Second, we anticipated that the expansion factors of the observed field lines should more closely match the larger values predicted by the model solutions with the added flux than those without it; however, we found that while the analysis could not differentiate between the two possibilities, neither were out of observational bounds.

In retrospect, it is not surprising that our analysis of the expansion factors of coronal magnetic field lines was not able to distinguish between the "no-flux-added" and "flux-added" solutions. First, even between the two model solutions, the expansion factors are not neatly separated into two clear groups (compare the vertical separation of the green and red circles in Figure 8). Second, there is likely significant noise introduced in the estimation of the expansion factors of the "observed" field lines. In fact, these white-light rays are only an approximate trace of what we believe are field lines laying underneath the plasma. In addition, they may not be exactly located in the plane of the sky. Finally, the digitation procedure itself likely introduces a nonnegligible noise component. It is worth noting, however, that this is, we believe, the first time that expansion factors have been estimated from white-light observations, and these estimates are, to a large extent, consistent with values obtained from our global MHD model.

Our results suggest that there may be no need to apply ad hoc corrections to the photospheric data, such as were advocated by Wang & Sheeley (1995). They first suggested that the photospheric field images produced by the Wilcox Solar Observatory (WSO) were quantitatively incorrect, arguing that rather than multiplying pixels by the suggested correction for WSO, the correction procedure derived for measurements at Mount Wilson Observatory (MWO) should instead be applied. They showed that the otherwise significant disagreement between measured 1 au values of the IMF and those extrapolated out to 1 au using a Potential Field Source-Surface (PFSS) model could be largely resolved by applying this correction factor. However, its use could not be defended theoretically, and, was disputed by researchers from WSO (Svalgaard 2006) as well as others (Riley 2007; Riley et al. 2014). We believe it was more of a pragmatic solution to bring the solar and interplanetary measurements into agreement. Instead, we tentatively suggest that the open flux problem may be resolved (at least in part) by adding a modest polar flux to photospheric magnetic field maps to correct for this deficit. The amount and spatial distribution, however, remain to be estimated. The values given here are probably reasonable for solar minimum conditions, but may also be limited to the minimum conditions surrounding 2008, which served as the period over which our analysis centered. By estimating the relative offset of the "missing" flux between models and observations (Riley 2007), it should be possible to prescribe the necessary polar flux correction as a function of solar cycle.

Our study did not address a second possible solution to the open flux problem proposed by Linker et al. (2017), namely that a large fraction of open flux may not be rooted within regions that are dark in emission (e.g., Lowder et al. 2017; Wallace et al. 2019). Generally, it is believed that dark regions correspond to open fields, while bright regions trace closed loops. It is through comparisons of such images with computed coronal hole boundaries that leads to the constraints on how large modeled coronal holes can be. However, projection of bright loops at the edges of coronal holes could act to reduce the observed size of coronal holes. Similarly, small patches of open field near otherwise closed regions, such as near active regions, may not register as being open in the sense that they do not produce coherent dark regions, yet may add to the open flux in the heliosphere. Linker et al. (2017) compared simulated EUV maps with computed coronal hole areas, concluding that, at least for steady-state solutions, the under-detection of coronal hole areas contributes only a small fraction to the total open flux.

A third, and, at least superficially appealing alternative explanation for this "missing" flux is that all solar observatories have substantially underestimated the strength of the photospheric magnetic field (by a factor of two or more). An argument for this could be made based on the countless examples of where corrections for both ground-based and space-based measurements have been introduced during the course of observations (Riley et al. 2014). The support for such adjustments is generally based on the fact that a new observatory was producing results that did not match either measurements from a different, more established observatory, or from a discrepancy introduced following an instrumental upgrade. However, there have been a sufficient number of independent developments in solar optics over the years that such a scenario seems unlikely. Moreover, the discrepancies found are generally less than ~50%, not the factor of two or more that appears to be required (Riley et al. 2014). Finally, it seems unlikely every observatory would systematically underestimate, and never overestimate, the photospheric values.

Several avenues of research could be pursued to test this idea further. For example, here, we have focused on solar minimum candidates because of their simplicity and that the effect is likely to be more pronounced. At solar maximum, when the near-axial symmetry of the flux distribution is broken, particularly at the time of solar field reversal (Riley et al. 2002, 2003), this effect would be minimized or not exist at all. Of course, such active conditions are intrinsically more difficult to model; thus, it may not be possible to identify systematic offsets in streamer stalks even if they existed. Another implication relates to the impact that such a distribution would have on flux transport and/or dynamo models. Some flux transport models, in fact, already support the idea of there being concentrated bundles of unipolar flux at high polar latitudes. The ADAPT model, in particular, generates synoptic maps, that preserve one sign of active region fields as they drift

meridionally poleward (Arge et al. 2010). It should be noted, however, that Wallace et al. (2019) recently compared estimates for the open magnetic flux using traditional diachronic maps and ADAPT synchronic maps finding, however, that the ADAPT solutions were unable to improve the deficit in the model estimates when compared with in situ measurements.

The effects of these polar fluxes could also be explored by adding them to other global models of the solar corona and inner heliosphere, such as WSA+Enlil or CORHEL, both of which can be run as NASA's CCMC. Does the additional polar flux improve model predictions for, say, the phasing of sector boundary crossings or solar wind speed at 1 au (e.g., Riley et al. 2015)?.

Finally, it would be worth pursuing other possible explanations to resolve the open flux problem. Although, as we have noted, it appears that steady-state solutions cannot "hide" sufficient coronal hole area in simulated EUV images, it may be possible that the added complexity and ongoing reconfiguration of time-dependent coronal magnetic fields might both add additional flux while also hiding it from view, at least with currently available observations. Thus, a careful analysis of long-period, time-dependent global MHD simulations might result in larger values of the open flux at 1 au without producing large-scale coronal holes that are in obvious disagreement with observations.

Ultimately, ESA's upcoming *Solar Orbiter* mission may be able to refute or validate these predictions. With a maximum extent of 34° during its extended mission, these bundles of concentrated flux should be clearly visible. The payload will include the remote sensing instrument, Polarimetric and Helioseismic Imager (PHI), which will provide accurate estimates of the photospheric magnetic field over the polar regions, as well as the in situ Magnetometer instrument (MAG), which will provide simultaneous measurements of the IMF.

We would like to acknowledge NASA's Living with a Star program (grant No.: NNX15AF39G), the Heliophysics Guest Investigator program (grant No.: NNX17AB78G), Heliophysics Supporting Research program (grant No.: 80NSSC18K0101), the joint NASA/NOAA O2R program (grant No.: NA18NWS4680081), and the Air Force Office of Scientific Research (Contract Number: FA9550-15-C-0001). We also acknowledge use of NASA/GSFC's Space Physics Data Facility's COHOWeb service (http://omniweb.sci.gsfc.nasa.gov/coho/) in retrieving the OMNI_M data, as well as supercomputing resources provided by NASA's Advanced Supercomputing Division (Pleiades) and NSF's XSEDE program (Comet).

ORCID iDs

Zoran Mikic https://orcid.org/0000-0002-3164-930X
Ronald M. Caplan https://orcid.org/0000-0002-2633-4290
Cooper Downs https://orcid.org/0000-0003-1759-4354

References

Arge, C. N., Henney, C. J., Koller, J., et al. 2010, in AIP Conf. Proc. 1216, Twelfth Int. Solar Wind Conf., ed. M. Maksimovic et al. (Melville, NY: AIP), 343
Balogh, A., Gonzalez-Espara, J. A., Forsyth, R. J., et al. 1995, SSRv, 72, 171
Caplan, R., Downs, C., & Linker, J. 2016, ApJ, 823, 53
Caplan, R. M., Mikic, Z., & Linker, J. A. 2017, arXiv:1709.01126
Caplan, R. M., Mikić, Z., Linker, J. A., & Lionello, R. 2017, JPhCS, 837, 012016
Gosling, J. T. 1997, in Coronal Mass Ejections, ed. N. Crooker, J. A. Joselyn, & J. Feynman, Vol. 99 (Washington, DC: AGU), 9
Habbal, S. R., Druckmüller, M., Morgan, H., et al. 2011, ApJ, 734, 120
Hoeksema, J. T., Wilcox, J. M., & Scherrer, P. H. 1983, JGR, 88, 9910
Ito, H., Tsuneta, S., Shiota, D., Tokumaru, M., & Fujiki, K. 2010, Ap.J., 719, 131
Linker, J., Caplan, R., Downs, C., et al. 2017, ApJ, 848, 70
Linker, J. A., & Mikić, Z. 1997, in Coronal Mass Ejections, ed. N. Crooker, J. A. Joselyn, & J. Feynman, Vol. 99 (Washington, DC: AGU), 269
Linker, J. A., Mikić, Z., Bisecker, D. A., et al. 1999, JGR, 104, 9809
Linker, J. A., Mikic, Z., Riley, P., et al. 2012, in AIP Conf. Proc. 1539, Proc Solar Wind 13, ed. G. P. Zankand et al. (Melville, NY: AIP), 26
Lionello, R., Linker, J. A., & Mikić, Z. 2009, ApJ, 690, 902
Lionello, R., Mikić, Z., & Linker, J. A. 1999, JCoPh, 152, 346
Lowder, C., Qiu, J., & Leamon, R. 2017, SoPh, 292, 18
Mikić, Z., & Linker, J. A. 1994, ApJ, 430, 898
Mikić, Z., Linker, J. A., Schnack, D. D., Lionello, R., & Tarditi, A. 1999, PhPl, 6, 2217
Okunev, O. V., & Kneer, F. 2004, A&A, 425, 321
PSI, 2019, Predictive Science Modeling Support for STEREO and SECCHI, https://www.predsci.com/stereo/home.php
Riley, P. 2007, ApJL, 667, L97
Riley, P., Ben-Nun, M., Linker, J., et al. 2014, SoPh, 289, 769
Riley, P., Ben-Nun, M., Linker, J. A., et al. 2014, SoPh, 289, 769
Riley, P., Linker, J. A., & Arge, C. N. 2015, SpWea, 13, 154
Riley, P., Linker, J. A., Lionello, R., & Mikic, Z. 2012, JASTP, 83, 1
Riley, P., Linker, J. A., & Mikić, Z. 2001, JGR, 106, 15889
Riley, P., Linker, J. A., & Mikić, Z. 2002, JGRA, 107, 1136
Riley, P., Linker, J. A., Mikić, Z., et al. 2006, ApJ, 653, 1510
Riley, P., Lionello, R., Mikić, Z., & Linker, J. 2008, ApJ, 672, 1221
Riley, P., Mikić, Z., & Linker, J. A. 2003, AnGeo, 21, 1347
Scherrer, P. H., Bogart, R. S., Bush, R. I., et al. 1995, SoPh, 162, 129
Svalgaard, L. 2006, A Floor in the Open Flux IMF Strength Constant in Time (Centuries) and Space (Latitude), in AGU Fall Meeting (Washington, DC: AGU), SH21A-0313
Tsuneta, S., Ichimoto, K., Katsukawa, Y., et al. 2008, Ap.J., 688, 1374
Wallace, S., Arge, C., Pattichis, M., Hock-Mysliwiec, R., & Henney, C. 2019, SoPh, 294, 19
Wang, Y.-M., & Sheeley, N., Jr 1995, ApJL, 447, L143